

PACE: A Large-Scale Dataset with Pose Annotations in Cluttered Environments

Yang You^{1,3*} Kai Xiong¹ Zhening Yang² Zhengxiang Huang¹
Junwei Zhou¹ Ruoxi Shi¹ Zhou Fang¹
Adam W. Harley³ Leonidas Guibas³ Cewu Lu^{1**}

¹ Shanghai Jiao Tong University

² Horizon Robotics Inc.

³ Stanford University

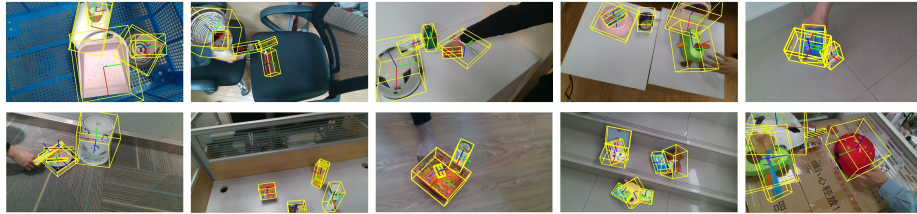


Fig. 1: We propose PACE: a large-scale object pose dataset, with diverse objects, complex scenes, and various types of occlusions. These samples highlight the dataset’s relevance to pose estimation challenges in the real world, where occlusions and clutter are common.

Abstract. Pose estimation is a crucial task in computer vision and robotics, enabling the tracking and manipulation of objects in images or videos. While several datasets exist for pose estimation, there is a lack of large-scale datasets specifically focusing on cluttered scenes with occlusions. We introduce PACE (Pose Annotations in Cluttered Environments), a large-scale benchmark designed to advance the development and evaluation of pose estimation methods in cluttered scenarios. PACE consists of 54,945 frames with 257,673 annotations across 300 videos, covering 576 objects from 44 categories and featuring a mix of rigid and articulated items in cluttered scenes. To annotate the real-world data efficiently, we developed an innovative annotation system utilizing a calibrated 3-camera setup. We test state-of-the-art algorithms in PACE along two tracks: pose estimation, and object pose tracking, revealing the benchmark’s challenges and research opportunities. Our code and data will be publicly available.

1 Introduction

The field of 3D object pose estimation is integral to a myriad of applications, particularly within robotic manipulation. Recent advancements in both instance and

* Work done at Shanghai Jiao Tong University.

** Cewu Lu is the corresponding author. Email: lucwu@sjtu.edu.cn

category-level pose estimation have been bolstered by deep learning approaches, and perhaps more importantly, by *data*.

PoseCNN [40] advanced pose estimation into the deep learning era, and simultaneously introduced the influential YCB-Video dataset. This benchmark has catalyzed methodological development and offered a consistent evaluation platform. Additionally, the Benchmark for 6D Object Pose Estimation (BOP) challenges have consolidated datasets and refined evaluation metrics for instance-level pose estimation.

In parallel, NOCS [36] has addressed category-level pose estimation, albeit with a smaller real-world dataset for validation and testing. Despite these strides, the field grapples with a fundamental challenge: state-of-the-art pose estimation models still perform poorly in real-world settings, and existing evaluation datasets are too constrained to thoroughly reveal this fact. The NOCS REAL275 dataset, for instance, spans only six categories and includes a mere 18 videos. This limitation has led to an array of published models which perform near-perfectly on NOCS but do not generalize to new data, as demonstrated in Figure 2.

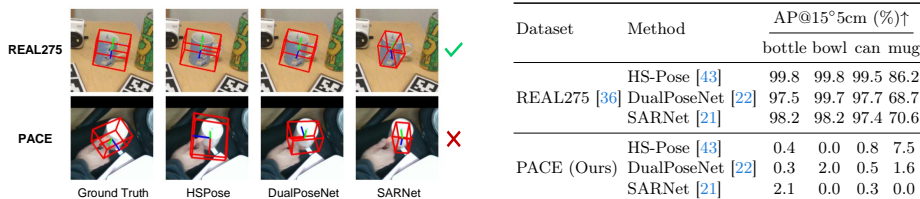


Fig. 2: While current state-of-the-art methods yield satisfactory outcomes on the NOCS REAL275 dataset, their models’ performance significantly deteriorates when transferred to previously unseen datasets such as PACE. **Left:** Qualitative visualizations of various models’ pose predictions for a mug in REAL275 vs. a mug in PACE. **Right:** The performance of state-of-the-art methods markedly declines on PACE, even when evaluating on categories that exist in both datasets.

In this work, we introduce PACE, a benchmark for pose estimation, and present a comprehensive study evaluating a wide range of pose estimation and tracking methods. Our contributions are threefold:

- **The PACE dataset:** This dataset includes 576 objects across 44 categories, captured in 300 video clips within diverse scenes. With an average of 183 frames per clip, the dataset consists of 54,945 frames and 257,673 annotations, providing a large-scale benchmark for pose estimation.
- **Our evaluation study:** To the best of our knowledge, we are the first to analyze and report the performance of state-of-the-art (SOTA) pose estimation methods in a large-scale cluttered setting. These results provide valuable insights on the scalability and generalizability of SOTA methods, making it clear that they are far from reliable in general.
- **Our annotation pipeline:** We will open-source our annotation pipeline, which uses a calibrated 3-camera system, enhancing the precision and scalability of annotating poses in real data. This tool significantly mitigates human

error and reduces the effort required for annotating 3D poses, providing a solution to one of the major bottlenecks in pose dataset creation.

Overall, our work aims to support the development of more robust and generalizable pose estimation techniques, thereby facilitating progress towards successful pose estimation in the real world.

2 Related Works

The field of 3D object pose estimation has seen substantial progress over the past few years. This progress has been facilitated by the introduction of standardized datasets and the development of innovative algorithms.

2.1 Object Pose Datasets

Instance-Level Pose Datasets YCB-Video dataset [40] is a comprehensive resource for 6D object pose estimation, containing a large number of video frames with accurate pose annotations for 21 objects. LINEMOD-Occluded [3] offers a challenging setting for pose estimation with piled multiple objects in occluded scenes. NAVI dataset [15] presents casually captured images of objects with high-quality 3D scans and precise 2D-3D alignments for 3D reconstruction tasks.

Category-Level Pose Datasets CO3D [27] offers 1.5 million frames from nearly 19,000 videos across 50 MS-COCO categories for category-specific 3D reconstruction and view synthesis. The Scan2CAD [2] dataset aligns 14225 CAD models from ShapeNet to 1506 ScanNet scans, promoting CAD model alignment in RGB-D scans. Pix3D [31] is a benchmark with image-shape pairs and pixel-level 2D-3D alignment, aiding in shape reconstruction and retrieval. The HOI-4D dataset [25], with 2.4M RGB-D frames over 4000 sequences, enables research in category-level human-object interaction. HANDAL [11] focuses on pose estimation and affordance prediction for robotics-ready manipulable objects. Table 1 presents a comparative comparison of these datasets, alongside our new dataset PACE.

2.2 Pose Estimation Methods

Instance-level Pose Estimation PPF (Point Pair Features) [8] sets the pre-deep learning standard for instance-level pose estimation, utilizing local geometric features from point clouds. The deep learning era began with PoseCNN [40], leading to several advanced methods. DeepIM [20] approaches pose estimation as an image matching task, iteratively refining estimations. DenseFusion [34] combines global and local features for pose estimation in cluttered scenes, while CosyPose [18] integrates a global refinement strategy in its end-to-end pipeline. SurfEmb [12] leverages surface embeddings for correspondence matching, and GDRNPP [35] employs geometry-guided regression for enhanced prediction.

	Modality	Cat.	Obj.	Vid.	Img.	Anno.	CAD	Dyn.	Occ.	Marker-free	Artic.	Piled
YCB-Video [40]	RGBD	-	21	12	20K	99K	✓	✗	✓	✓	✗	✓
LINEMOD-O [3]	RGBD	-	8	1	1.2K	9.2K	✓	✗	✓	✗	✗	✓
NAVI [15]	RGBD	-	36	324	10K	10k	✓	✗	✗	✓	✗	✗
NOCS-REAL275 [36]	RGBD	6	42	18	8K		✓	✗	✓	✗	✗	✗
Wild6D [42]	RGBD	5	1722	5166	1.1M	1.1M	✗	✗	✗	✓	✗	✗
Objectron [1]	RGB	9	17k	14k	4M	4M	✗	✗	✗	✓	✗	✗
CO3D [27]	RGB	50	19K	19K	1.5M	1.5M	✓	✗	✗	✓	✗	✗
Scan2CAD [2]	RGBD	9	3K	1506	-	14K	✓	✗	✓	✓	✗	✗
Pix3D [31]	RGBD	9	395	-	10K	10K	✓	✗	✗	✓	✗	✗
HOI-4D [25]	RGBD	16	800	4K	2.4M	-	✓	✓	✓	✓	✓	✗
HANDAL [11]	RGB	17	212	2K	308K	308K	✓	✓	✓	✓	✗	✗
PACE (Ours)	RGBD	44	576	300	55K	258K	✓	✓	✓	✓	✓	✓

Table 1: Comparison of object pose datasets. From left to right, the table captures input modality, number of categories, number of instances, number of videos, number of images, number of total annotations, whether 3D CAD models are provided, whether videos include static and/or dynamic moving objects, whether objects are occluded in some frames, whether images contain artificial markers, whether poses for each part of articulated objects are provided, and whether multiple objects are piled in some frames. Compared with most other datasets, PACE contains dynamic and articulated objects.

Category-level Pose Estimation Category-level pose estimation extends the challenge to generic object categories. NOCS [36] introduces a unified coordinate space for all objects, predicting object NOCS maps from RGB images. SGPA [4] aims to adapt the structure-guided prior in the pose estimation process, while SAR-Net [21] uses shape alignment and symmetric correspondence to estimate a coarse 3D object shape and facilitate object center and size estimation. Recently, HS-Pose [43] proposes a network structure with a HS-layer that extends 3D graph convolution to extract hybrid scope latent features from point clouds for category-level object pose estimation.

2.3 Pose Tracking Methods

Instance-level Pose Tracking Methods like RBOT [32] use RGB data and 3D models to track multiple objects, employing color histograms in their cost function. PoseRBPF [5] separates rotation and translation, using an autoencoder for rotation feature embeddings. ICG [30] iteratively refines pose using geometric cues and is effective for textureless objects, with extensions incorporating visual data [29]. The first deep learning tracker, D6DT [9], and se(3)-TrackNet [38] predict frame-to-frame relative poses, using a render-and-compare strategy.

Category-level Pose Tracking 6-PACK [33] performs category-level tracking, using DenseFusion [34] features and an attention mechanism for unsupervised keypoint ordering and interframe motion via keypoint matching. CenterPoseTrack [23] projects 2D keypoints from 3D bounding box vertices, achieving RGB-based scale-invariant tracking. BundleTrack [37] generalizes pose tracking without relying on 3D models, instead using video segmentation and pose graph

optimization. CAPTRA [39] tracks 9DoF poses for rigid and articulated objects, with subnetworks for rotation regression and normalized coordinate prediction, facilitating analytical 3D size and translation computation.

3 Construction of PACE

A key contribution of this work is the establishment of a **scalable** and **reliable** annotation framework, enabling the collection of large-scale and accurate pose annotations. An overview of the pipeline is depicted in Figure 3.

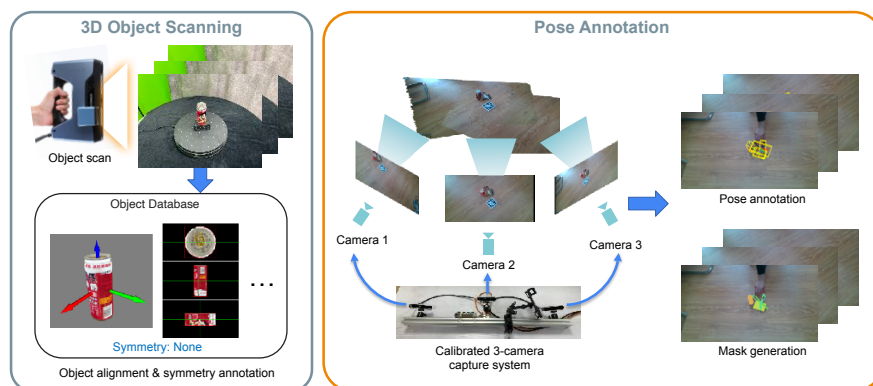


Fig. 3: Overview of the PACE annotation pipeline.

3.1 Acquisition of 3D Scans of Common Objects

We began by digitizing an extensive collection of commonplace objects. These items were categorized into 44 distinct classes, as represented in Figure 5. The Einscan Pro 2X was utilized for rapid scanning of all objects, typically completing within 5 to 10 minutes per object. To expedite this process, we employed a rotatable platform to acquire multiple viewpoints of objects. After scanning, objects were manually aligned to a standard pose within a uniform coordinate system. For each object, we centered its axis-aligned bounding box at the origin and then aligned the bounding box orientation along a common axis within the category. We additionally annotated rotational symmetries. High-resolution meshes were simplified to lower-resolution ones for a smoother annotation workflow.

Articulated Objects Diverging from many prior pose estimation datasets, our collection encompasses a very wide set of objects, including **articulated objects** from the AKB48 [24] dataset, namely: scissors, cutters, clips, and boxes. We adopt the alignment methodology from the original AKB48 dataset, without modification. These objects are segmented into multiple parts with hierarchical relationships, presenting a difficult challenge for pose estimation.

3.2 RGB-D Sequence Acquisition

We designed and implemented a 3-camera system to aid in data acquisition and annotation, comprising three Intel Realsense D415 RGB-D cameras affixed to a metal framework, as illustrated in the bottom of Figure 3. The advantages of this setup include:

- Tripling the data yield.
- Reducing ambiguity in pose annotation, especially regarding translation along the depth dimension, by enforcing annotation consistency across all 3 views.
- Enhancing tracking accuracy of static objects with ArUco markers [10] from all three views, making PnP more stable.

Calibration of Multi-Camera Extrinsic Parameters We calibrated this multi-camera system through a semi-automatic process. ArUco markers [10] alone proved insufficient for high-accuracy rotation estimation. Hence, we resorted to trifocal tensor estimation, i.e. TFT [16]. The process begins with feature extraction and matching, followed by bundle adjustment to refine the positions of the 3D landmarks and camera poses. For reliable feature matching, we employed the SuperPoint [7] descriptor and SuperGlue [28] matcher, using a stringent threshold for matching. We observed that rotational component of the resulting extrinsic parameters is precise, but the translation aspect suffers from scale ambiguity inherent in Structure-from-Motion approaches. We corrected this by calibrating the scale against markers, applying the following formula to obtain the optimal scale factor, by setting gradient of $\|s\hat{\mathbf{t}} - \mathbf{t}'\|_2^2$ to zero:

$$s_{1\rightarrow 2} = \frac{\hat{\mathbf{t}}_{1\rightarrow 2} \cdot \mathbf{t}'_{1\rightarrow 2}}{\hat{\mathbf{t}}_{1\rightarrow 2} \cdot \hat{\mathbf{t}}_{1\rightarrow 2}}, s_{1\rightarrow 3} = \frac{\hat{\mathbf{t}}_{1\rightarrow 3} \cdot \mathbf{t}'_{1\rightarrow 3}}{\hat{\mathbf{t}}_{1\rightarrow 3} \cdot \hat{\mathbf{t}}_{1\rightarrow 3}},$$

where $\hat{\mathbf{t}}_{i\rightarrow j}$ is the TFT predicted translation (up to a scale) from camera i to camera j , $\mathbf{t}'_{i\rightarrow j}$ is the marker-calibrated translation in real metric scale. We set the extrinsics of the first camera to be the identity matrix. We use Intel’s dynamic calibration tool to calibrate intrinsics.

In cases of repetitive texture patterns, we manually intervened to establish reliable correspondences, due to the limitations of SuperPoint+SuperGlue.

3.3 Annotation of Pose Ground-Truths

Previous methodologies have utilized ArUco markers to automate pose estimation through Perspective-n-Points, and we do this also. Specifically, we employed ArUco markers to automate the annotation of *static object* poses, following LINEMOD [3] and NOCS [36]. We note that this step has two limitations, which have plagued prior works:

1. Markers in the scene detract from realism and compromise dataset integrity: training on marker-augmented imagery may result in overfitting to these artificial patterns.

- Marker-based annotations are inapplicable to dynamic objects (since the markers are typically placed on the background), thus limiting the setup to annotating static objects.

We compensate for both of these issues: we remove marker appearances from the dataset (after using them for annotation), and we introduce additional tools to annotate the dynamic objects. We describe these compensation steps next.

Marker removal We removed the marker appearances from the dataset, using a marker inpainting strategy, detailed as follows. In step 1, we place a marker (Marker 1) somewhere within the camera’s field of view. We then record a short video with this marker in view. In step 2, we place a second marker (Marker 2) at a chosen distance from the first, and record another video. In step 3, we remove Marker 1, and begin the *actual* object capture process (with only Marker 2 present). After this process, we end up with: (1) frames with Marker 1 only, which clearly depict the surface where Marker 2 will later appear; (2) frames capturing both markers, providing helpful calibration cues; (3) frames with Marker 2 only, which represent our main capture. We leverage Marker 2 for automated pose tracking, and manually correct the tracking every 40 frames in case of drift. We use the frames from the first two steps to seamlessly inpaint [26] Marker 2’s area for the final dataset, as depicted in Figure 4.

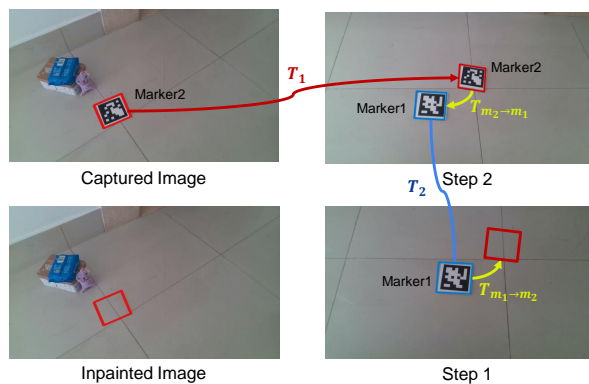


Fig. 4: Illustration of the marker inpainting process.

Annotation of Dynamic Object Poses For dynamic objects, the traditional marker-based tracking approach is insufficient, as the scene markers do not move in tandem with the objects. In such instances, we harnessed the capabilities of BundleTrack [37], an advanced RGB image-based tracking algorithm. BundleTrack conducts feature correspondence analysis between successive frames to estimate poses, complemented by a bundle adjustment algorithm to optimize keyframes globally and minimize tracking errors. Despite BundleTrack’s proficiency in approximating poses, it is prone to drift, necessitating the manual adjustment of poses every ten frames to ensure precision. We adopted a rigorous manual checking process, examining every tenth frame for 3D pointcloud

alignment and 2D multi-view agreement. We detail the annotation tool and its graphical interface in the supplementary. This delicate process represents the most labor-intensive aspect of our annotation pipeline.

In order to verify that our annotation process gives highly accurate poses, we conducted an experiment where we used our setup to manually annotate the poses of 1000 synthetic objects (for which we have exact ground truth), randomly sampling these objects from the synthetic part of our dataset (detailed in Section 4.3). We recorded an average pose annotation error of 0.88° for rotation and 1.2mm for translation, which is far below the estimation error of current models. More details of this experiment can be found in our supplementary.

Generation of Segmentation Masks Upon successful pose annotation, we generated occlusion-aware segmentation masks, via depth rendering. In cases where hand interactions are involved, we employed the segmentation model SAM [17] to estimate hand masks, and subsequently subtracted these from the previously computed object masks to obtain the occlusion-aware segmentation.

4 Dataset Statistics

In pursuit of diversity, we placed the objects in ten disparate environments, each featuring varying levels and configurations of occlusion. We captured 10 video sequences per scene, each sequence including 1 to 7 objects. We captured RGB and depth data using an Intel RealSense D415 camera, with a resolution of 1280×720 . The capture process spans distances ranging from 0.5m to 1.5m.

4.1 Object Distribution and Diversity

The comprehensive distribution of objects is depicted in Figure 5, showcasing a diverse array of both rigid and articulated models. As demonstrated in Figure 7, the dataset encompasses a broad spectrum of object sizes, with the majority measuring near 0.2m along the bounding box diagonal. It also includes larger items such as storage bins, adding to the heterogeneity of the dataset.

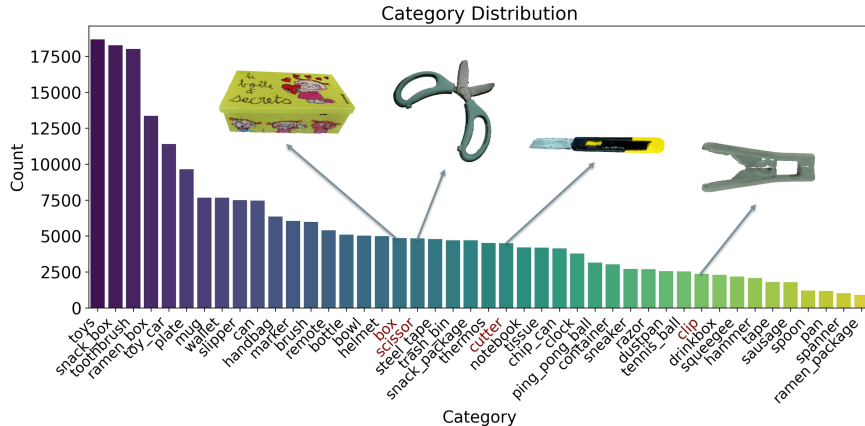


Fig. 5: Distribution of pose annotations with different object categories.

4.2 Variability in Pose, Occlusion, and Environmental Context

The dataset has rich variability in object poses, as illustrated in Figure 6, which outlines the statistical distribution of azimuth and elevation angles, indicating comprehensive spatial coverage.

We categorized and analyzed the occlusion levels, as shown in Figure 8, showing examples of severe, moderate, and minor occlusions. Organizing the data into these categories is helpful for assessing the robustness of pose estimation algorithms against varying degrees of visibility.

The ten distinct environments are shown in Figure 9, illustrating the diversity of backgrounds and lighting conditions.

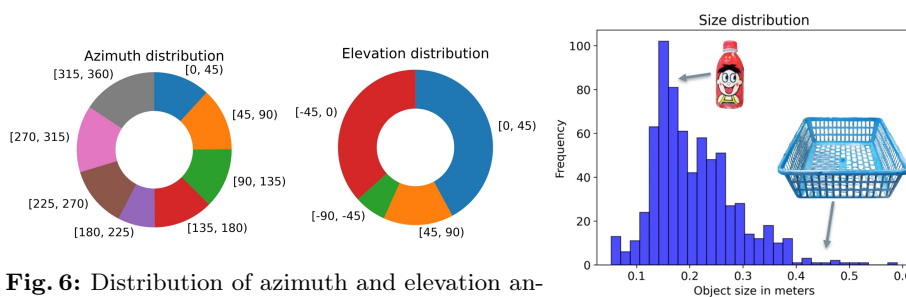


Fig. 6: Distribution of azimuth and elevation angles.

Fig. 7: Distribution of object sizes.

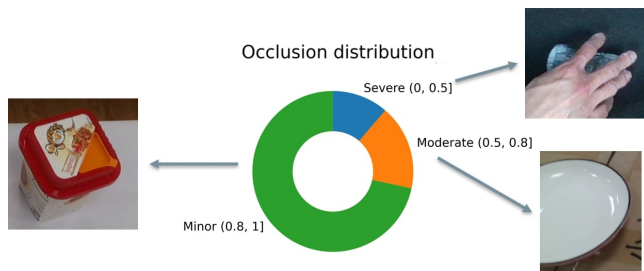


Fig. 8: Distribution of occlusion levels.

4.3 Dataset Split for Training, Validation, and Testing

To facilitate a comprehensive and equitable evaluation of pose estimation methodologies, we partitioned the (entirely real-world) dataset into validation and test subsets following a 20/80 ratio. This separation ensures that the main volume of the data is used for benchmarking (rather than for tuning hyperparameters).

Additionally, to support research necessitating extensive training datasets, **we generated a large synthetic dataset to be used as a training set.** Our synthetic dataset uses a physically based renderer [6] and is highly photo-realistic.

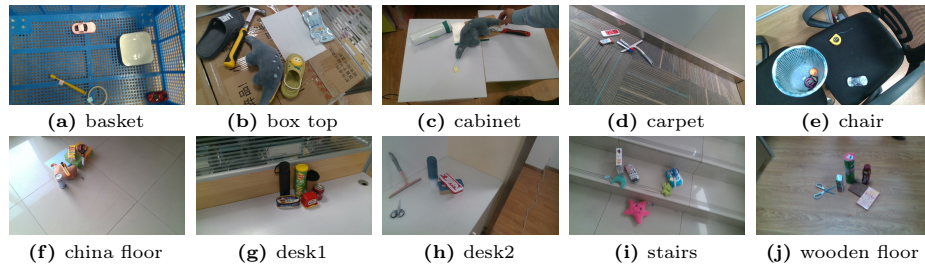


Fig. 9: Sample images from the 10 environments.

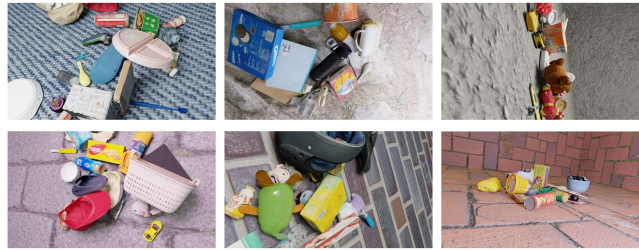


Fig. 10: Example images generated with the physically based renderer.

The training set consists of more than 52,000 images, each featuring dozens of objects, yielding a vast number of annotations. Qualitative examples of the synthetic images are presented in Figure 10.

5 Evaluation Benchmarks

We evaluate pose estimation, and pose tracking. State-of-the-art (SOTA) pose estimation algorithms typically decompose the task of pose estimation into two distinct stages: detecting or segmenting the object of interest, followed by pose estimation within the predicted bounding box or mask. We therefore examine pose estimation results under the assumption of perfect detection to allow for fair comparison across methods. The object detection performance of current SOTA methods can be found in the supplementary and is not the focus of this dataset. We evaluate instance-level and category-level pose estimators on our benchmark, and also provide an analysis of the failure modes.

To benchmark pose tracking, we indicate what to track by providing ground-truth data in the first frame of a video, and ask methods to propagate the ground truth to follow rotations and translations of the object in the video. We evaluate model-free and model-based pose trackers in this setup.

5.1 Pose Estimation Benchmark

This benchmark is divided into instance-level and category-level pose estimation. The former concerns object instances seen during training (in different scenes), while the latter concerns instances which were not seen but come from the same category. We will also give an in-depth analysis of failure modes of SOTA methods.

Instance-Level Pose Estimation This task demands the prediction of rotation and translation for known instances from the training set.

Metrics: Adhering to the BOP challenge protocol [14], we use Average Recall (AR) of Visible Surface Discrepancy (VSD), Maximum Symmetry-Aware Surface Distance (MSSD), and Maximum Symmetry-Aware Projection Distance (MSPD) as our metrics. Detailed computation of these metrics is described in [14]. Results are averaged across all instances.

Baselines: We assessed four baselines: PPF [8], CosyPose [18], SurfEmb [12], and GDRNPP [35]. While PPF does not require training data, the others are SOTA methods dependent on additional training on the PBR dataset. To focus on pose estimation performance, we assume that ground-truth detections are available.

Result Analysis: The quantitative analysis is presented in Table 2. Notably, while SOTA methods excel on the BOP benchmarks, they do not perform as well as PPF, which relies on local geometric feature matching in point clouds. The relative success of PPF highlights the potential for improvement in SOTA methods, particularly regarding sim-to-real ability and scalability to handle a large set of instances. Qualitative results can be found in the supplementary.

Modality Detection AR _{VSD} ↑ AR _{MSSD} ↑ AR _{MSPD} ↑ AR↑						
PPF [8]	D	G.T.	35.3	42.7	49.3	42.4
CosyPose [18]	RGB	G.T.	1.4	0.3	11.5	4.4
SurfEmb [12]	RGB	G.T.	6.2	3.0	17.8	9.0
GDRNPP [35]	RGB-D	G.T.	3.6	2.1	15.4	7.0

Table 2: Instance-level pose estimation results showcasing the robustness of PPF and the potential for improvement in SOTA deep learning-based methods.

	Detection	IoU ₂₅ ↑	IoU ₅₀ ↑	AP					
				0:20°↑	0:60°↑	0:5cm↑	0:15cm↑	0:20° 0:5cm↑	0:60° 0:15cm↑
NOCS [36]	Mask-RCNN	0.1/0.0	0.0/0.0	0.2/0.0	1.3/0.0	17.3/0.0	33.6/0.0	0.2/0.0	1.2/0.0
HS-Pose [43]	G.T.	38.5/0.2	7.9/0.0	5.2/0.0	6.9/0.4	58.8 /39.2	85.0 /78.2	3.8/0.0	6.4/0.4
SGPA [4]	G.T.	9.2/0.1	1.1/0.0	7.1/0.9	14.1/5.6	22.6/29.4	64.9/56.1	4.3/0.7	12.7/5.5
DualPoseNet [22]	G.T.	35.7/1.1	2.3/0.0	5.8/0.0	9.3/0.0	38.5/ 39.3	75.0/ 78.3	3.3/0.0	8.2/0.0
SAR-Net [21]	G.T.	27.1/0.1	1.4/0.0	5.2/0.0	6.6/1.3	45.6/41.0	80.3/71.0	3.1/0.0	5.9/1.3
CPPF++ [41]	G.T.	52.2 / 11.2	16.9 / 0.1	16.3 / 3.4	23.9 / 10.7	44.0/35.4	76.8/76.1	13.9 / 2.6	22.9 / 10.4
ANCSH [19]	G.T.	-/0.0	-/0.0	-/0.0	-/0.3	-/19.3	-/51.0	-/0.0	-/0.3

Table 3: Category-level pose estimation benchmark combining the performance metrics for both rigid and articulated object pose estimation, separated by slash.

Category-Level Pose Estimation Category-level pose estimation tasks involve predicting the 3D bounding box dimensions, rotation, and translation of target instances, given only the category information a priori.

Metrics: We adopted from NOCS [36], calculating mean Average Precision (AP) across predefined angle and translation thresholds. Specifically, AP@0:20° represents AP averaged from 0° to 20° at 1° intervals; AP@0:5cm is averaged from 0cm to 5cm at 0.25cm intervals; AP@0:20°,0:5cm combines these angle and translation thresholds. IoU₂₅ and IoU₅₀ denote AP for 3D bounding box matches at IoU thresholds of 25 and 50, respectively. Results are separately reported for both rigid and articulated objects.

Baselines: We evaluated seven recent category-level pose estimation methods: NOCS [36], HS-Pose [43], SGPA [4], DualPoseNet [22], SAR-Net [21], CPPF++ [41] and ANCSH [19], the latter specifically designed for articulated objects. For adapting rigid-object-focused methods to articulated objects, each movable part is considered a distinct category. For instance, scissors with two movable parts are treated as two separate categories. Ground-truth detections are presumed for each method, except for NOCS, which outputs both instance masks and pose estimations using a unified network.

Result Analysis: Quantitative comparisons are listed in Table 3. On rigid objects, HS-Pose and DualPoseNet show fair performance on AP metrics for translation, but falls short on rotation AP metrics compared to CPPF++, suggesting a proficiency in size and translation prediction but not rotation. CPPF++ shows the best performance but is weaker on translation estimation. For articulated objects, all methods face challenges due to the movable parts, with ANCSH underperforming on the large-scale real-world dataset, indicative of a significant sim-to-real gap. NOCS shows instability, likely due to its jointly outputting both the masks and poses, which lacks robustness and scalability. Qualitative results are available in supplementary.

Failure Mode Analysis This section delves into the analysis of two critical questions that underline the failure of SOTA deep learning-based methods in pose estimation: 1) Is the failure attributed to the sim-to-real gap, considering the exclusive use of synthetic RGB-D images for training? 2) Does the failure stem from the inherent large-scale complexity of the PACE dataset, which poses a significant challenge for baseline models?

Ablation Setup: To explore these questions, we introduced a new 80/10/10 train/validation/test split for the real-world data, diverging from the 0/20/80 split described in Section 4.3. We then examined the following settings:

- *Real2Real Single Instance/Category Fitting:* This basic setup involves training on a single instance or category selected (we randomly select the category *can* and sample a can with object ID 57) from the 80/10/10 split of real data.
- *Sim2Real Single Instance/Category Fitting:* This scenario differs from the first by utilizing all simulated data for training and validation, with evaluation on the same real-world test split.
- *Real2Real All Instance/Category Fitting:* Unlike the first setting, this involves training, validation, and testing across all instances or categories.

Training Setting	Instance-Level (AR%) [†]			Category-Level (mean AP%@0:60°, 0:15cm) [†]					
	CosyPose	SurfEmb	GDRNPP	NOCS	HS-Pose	SGPA	DualPoseNet	SAR-Net	CPPF++
Real2Real Single Inst./Cat.	76.4	86.7	88.2	76.9	81.2	86.7	58.6	59.3	83.4
Sim2Real Single Inst./Cat.	67.1 (-9.3↓)	73.7 (-13.0↓)	78.1 (-10.1↓)	55.8 (-21.1↓)	1.1 (-80.1↓)	0.3 (-86.4↓)	1.4 (-57.2↓)	33.2 (-26.1↓)	24.3 (-59.1↓)
Real2Real All Inst./Cat.	8.2 (-68.2↓)	11.2 (-75.5↓)	9.7 (-78.5↓)	0.3 (-76.6↓)	5.6 (-75.6↓)	9.8 (-76.9↓)	1.2 (-57.4↓)	2.1 (-57.2↓)	13.7 (-69.7↓)

Table 4: Ablation Study: This study illustrates the challenges models face when transitioning from real-to-real settings. It showcases performance disparities when scaling from single instances/categories to the entire dataset, emphasizing the scalability challenge from PACE and the profound impact of sim-to-real discrepancies on depth-dependent methodologies.

Result Analysis and Discussions: The findings presented in Table 4 shed light on several insights. The satisfactory performance under the *Real2Real Single Instance/Category Fitting* setting indicates that baseline models are inherently capable of fitting a single instance or category, provided the training and test data distributions are consistent.

The sim-to-real gap observed, particularly for specific methods, underscores the challenges faced in sim-to-real scenarios. The first two rows of Table 4 demonstrate that, although all methods perform adequately with real training data, their efficacy diminishes in sim-to-real transitions. Depth-input methods, such as DualPoseNet, HS-Pose, and SGPA, face a much larger sim-to-real gap than RGB-input methods, largely due to the challenges in simulating depth noise. Our supplementary materials further corroborate this, showing reasonable object detection performance in sim-to-real settings with RGB only.

Moreover, the task of learning across all instances/categories is challenging for all models. There is a dramatic decline in performance when extending the scope to all instances/categories, as observed in the third row of Table 4. We also observed suboptimal training data performance and loss plateauing despite prolonged training, which points to model underfitting. These outcomes suggest that the intrinsic vastness and diversity posed by PACE are significant contributors to the underwhelming performance of SOTA models.

Addressing these failures may require innovative techniques to bridge the sim-to-real gap by reconciling depth discrepancies or the development of larger foundational models capable of managing the diversity and vastness in the real-world data.

5.2 Pose Tracking Benchmark

We categorize SOTA pose tracking methods into model-based, which use a 3D CAD model, and model-free, requiring only the initial pose at the first frame.

Metrics: For model-free pose tracking, we used four metrics following previous work [33]. 1) **5°5cm**, the percentage of predictions with rotation error $< 5^\circ$ and translation error $< 5\text{cm}$. 2) **IoU25**, the percentage of intersection over union that is larger than 25% between the two 3D bounding boxes with ground-truth size, transformed by the predicted and ground-truth 6D pose, respectively. 3) **R_{err}**, mean value of rotation error in degrees. 4) **T_{err}**, mean value of translation

error in centimeters. Here the last two metrics are respect to IoU25 since objects with $\text{IoU} \leq 25\%$ are not counted.

For model-based pose tracking, we reported the area under curve (AUC) with respect to ADD, ADD-S [40] and ADD(-S). We set the maximum threshold of AUC to be 0.1m [34]. The ADD metric is first introduced in [13] to calculate average per-point distance between two point clouds, transformed by the predicted pose and the ground-truth, respectively. For symmetric objects like bowls, ADD-S metric is introduced to count for the point correspondence ambiguity. The notation ADD(-S) corresponds to computing ADD for non-symmetric objects and ADD-S for symmetric objects. The objects with visibility fraction less than 10% are skipped for evaluation following the BOP [14] convention. Results are reported by averaging over the rigid/articulated categories, separately.

	Modality	ADD \uparrow	ADD-S \uparrow	ADD(-S) \uparrow
RBOT [32]	RGB	7.1/0.5	10.3/0.8	7.4/0.5
ICG [30]	RGB-D	35.6/10.1	48.1/15.2	38.1/10.1

Table 5: Model-Based Pose Tracking. We report the area under curve (AUC) with respect to ADD, ADD-S and ADD(-S). The higher value, the better performance.

	Training-Free	Modality	5 $^\circ$ 5cm \uparrow	IoU25 \uparrow	R $_{err}\downarrow$	T $_{err}\downarrow$
BundleTrack [37]	\checkmark	RGB	6.4/ 11.2	9.1/14.1	3.2/5.5	2.6/ 0.8
CAPTRA [39]	\times	D	12.9/4.4	45.8/20.6	19.2/40.9	2.2/1.5
6-PACK [33]	\times	RGB-D	9.2/3.9	23.1/16.7	17.7/33.6	2.1/1.2

Table 6: Model-Free Pose Tracking. Both rigid and articulated results are reported. For 5 $^\circ$ 5cm and IoU25, the higher value means better performance while for R $_{err}$ and T $_{err}$, the situation is reversed. Note that R $_{err}$ and T $_{err}$ are respect to IoU25 since objects with $\text{IoU} \leq 25\%$ are not counted.

Baselines: For methods relying on object mask during tracking, we directly used the ground-truth mask. All tracking methods estimates the rotation and translation except for CAPTRA, which additionally estimates the 3D bounding box size. We still use the ground-truth bounding box size for a fair evaluation.

We regarded each part of the articulated objects as independent for all tracking methods except for CAPTRA [39] which treat all parts of an object as a whole. We trained CAPTRA for each category using our synthetic PBR data.

Result and Failure Mode Analysis: Tables 5 and 6 present the performance metrics of SOTA tracking methods on the PACE dataset with both rigid and articulated results separated by slash. SOTA methods exhibit limited success, with ICG [30] achieving the highest AUC with respect to ADD(-S) at only 38.1% for rigid objects and a mere 10.1% for articulated objects, as shown in Table 5. Table 6 underscores the challenge further, with the best 5 $^\circ$ 5cm accuracy below 13%, and IoU25 not exceeding 47%, indicating substantial pose estimation errors.

The convention followed by 6-PACK [33] and BundleTrack [37] disregards objects with $\text{IoU} \leq 25\%$ when computing rotational and translational errors

(R_{err} and T_{err}). However, in the context of our dataset where methods generally struggle, this approach could mask true performance levels. This discrepancy is exemplified by BundleTrack [37], which reports lower performance in $5^\circ 5\text{cm}$ and IoU25 metrics yet shows seemingly better results for R_{err} and T_{err} , suggesting that it can only track well within a threshold but cannot recover once the object is lost. Such results indicate that current SOTA methods may require significant improvements to handle the complexity presented by the PACE dataset effectively. Qualitative results can be found in the supplementary.

6 Conclusions and Limitations

We introduce PACE: Pose Annotations in Cluttered Environments, a comprehensive large-scale benchmark for 3D object pose estimation and tracking, featuring varying levels and configurations of occlusion, within ten diverse environments. This benchmark serves not only as a testament to the progress achieved in prior work but also as a call for the research community to address the complexities in real world. Our findings reveal that while there have been significant advancements in pose estimation techniques, there exists a substantial performance gap when these methods are applied to real-world settings such as those in PACE. Particularly, current SOTA methods struggle with articulated objects and exhibit limitations in robustness and scalability. To bridge this gap, future research could explore the potential of more advanced sim-to-real methodology, and larger models that can encapsulate a wider variety of object features and environmental contexts.

Limitations Our dataset does not contain large or valuable objects such as tables, cameras, and laptops, due to resource constraints. This potentially limits the dataset’s comprehensiveness and its applicability to certain objects in real-world scenes.

7 Acknowledgements

This work is supported by the National Key Research and Development Project of China (No. 2022ZD0160102), National Key Research and Development Project of China (No. 2021ZD0110704), Shanghai Artificial Intelligence Laboratory, XPLOER PRIZE grants. Yang You is also supported in part by the Outstanding Doctoral Graduates Development Scholarship of Shanghai Jiao Tong University.

References

1. Ahmadyan, A., Zhang, L., Ablavatski, A., Wei, J., Grundmann, M.: Objectron: A large scale dataset of object-centric videos in the wild with pose annotations. In: Proceedings of the IEEE/CVF conference on computer vision and pattern recognition. pp. 7822–7831 (2021) 4
2. Avetisyan, A., Dahnert, M., Dai, A., Savva, M., Chang, A.X., Nießner, M.: Scan2cad: Learning cad model alignment in rgb-d scans. In: Proceedings of the IEEE/CVF Conference on computer vision and pattern recognition. pp. 2614–2623 (2019) 3, 4

3. Brachmann, E., Krull, A., Michel, F., Gumhold, S., Shotton, J., Rother, C.: Learning 6d object pose estimation using 3d object coordinates. In: Computer Vision–ECCV 2014: 13th European Conference, Zurich, Switzerland, September 6–12, 2014, Proceedings, Part II 13. pp. 536–551. Springer (2014) [3](#), [4](#), [6](#)
4. Chen, K., Dou, Q.: Sgpa: Structure-guided prior adaptation for category-level 6d object pose estimation. In: Proceedings of the IEEE/CVF International Conference on Computer Vision. pp. 2773–2782 (2021) [4](#), [11](#), [12](#)
5. Deng, X., Mousavian, A., Xiang, Y., Xia, F., Bretl, T., Fox, D.: Poserbpf: A rao–blackwellized particle filter for 6-d object pose tracking. *IEEE Transactions on Robotics* **37**(5), 1328–1342 (2021) [4](#)
6. Denninger, M., Winkelbauer, D., Sundermeyer, M., Boerdijk, W., Knauer, M., Strobl, K.H., Humt, M., Triebel, R.: Blenderproc2: A procedural pipeline for photorealistic rendering. *Journal of Open Source Software* **8**(82), 4901 (2023). <https://doi.org/10.21105/joss.04901>, <https://doi.org/10.21105/joss.04901> [9](#)
7. DeTone, D., Malisiewicz, T., Rabinovich, A.: Superpoint: Self-supervised interest point detection and description. In: Proceedings of the IEEE conference on computer vision and pattern recognition workshops. pp. 224–236 (2018) [6](#)
8. Drost, B., Ulrich, M., Navab, N., Ilic, S.: Model globally, match locally: Efficient and robust 3d object recognition. In: 2010 IEEE computer society conference on computer vision and pattern recognition. pp. 998–1005. Ieee (2010) [3](#), [11](#)
9. Garon, M., Lalonde, J.F.: Deep 6-dof tracking. *IEEE transactions on visualization and computer graphics* **23**(11), 2410–2418 (2017) [4](#)
10. Garrido-Jurado, S., Muñoz-Salinas, R., Madrid-Cuevas, F.J., Marín-Jiménez, M.J.: Automatic generation and detection of highly reliable fiducial markers under occlusion. *Pattern Recognition* **47**(6), 2280–2292 (2014) [6](#)
11. Guo, A., Wen, B., Yuan, J., OTHERS: Handal: A dataset of real-world manipulable object categories with pose annotations, affordances, and reconstructions (2023), <https://arxiv.org/pdf/2308.01477.pdf> [3](#), [4](#)
12. Haugaard, R.L., Buch, A.G.: Surfemb: Dense and continuous correspondence distributions for object pose estimation with learnt surface embeddings. In: Proceedings of the IEEE/CVF Conference on Computer Vision and Pattern Recognition. pp. 6749–6758 (2022) [3](#), [11](#)
13. Hinterstoisser, S., Lepetit, V., Ilic, S., Holzer, S., Bradski, G., Konolige, K., Navab, N.: Model based training, detection and pose estimation of texture-less 3d objects in heavily cluttered scenes. In: Computer Vision–ACCV 2012: 11th Asian Conference on Computer Vision, Daejeon, Korea, November 5–9, 2012, Revised Selected Papers, Part I 11. pp. 548–562. Springer (2013) [14](#)
14. Hodañ, T., Sundermeyer, M., Drost, B., Labbé, Y., Brachmann, E., Michel, F., Rother, C., Matas, J.: Bop challenge 2020 on 6d object localization. In: Computer Vision–ECCV 2020 Workshops: Glasgow, UK, August 23–28, 2020, Proceedings, Part II 16. pp. 577–594. Springer (2020) [11](#), [14](#)
15. Jampani, V., Maninis, K.K., Engelhardt, A., Karpur, A., Truong, K., Sargent, K., Popov, S., Araujo, A., Martin-Brualla, R., Patel, K., et al.: Navi: Category-agnostic image collections with high-quality 3d shape and pose annotations. *arXiv preprint arXiv:2306.09109* (2023) [3](#), [4](#)
16. Julià, L.F., Monasse, P.: A critical review of the trifocal tensor estimation. In: Image and Video Technology: 8th Pacific-Rim Symposium, PSIVT 2017, Wuhan, China, November 20–24, 2017, Revised Selected Papers 8. pp. 337–349. Springer (2018) [6](#)

17. Kirillov, A., Mintun, E., Ravi, N., Mao, H., Rolland, C., Gustafson, L., Xiao, T., Whitehead, S., Berg, A.C., Lo, W.Y., et al.: Segment anything. arXiv preprint arXiv:2304.02643 (2023) [8](#)
18. Labbé, Y., Carpentier, J., Aubry, M., Sivic, J.: Cosypose: Consistent multi-view multi-object 6d pose estimation. In: Computer Vision–ECCV 2020: 16th European Conference, Glasgow, UK, August 23–28, 2020, Proceedings, Part XVII 16. pp. 574–591. Springer (2020) [3](#), [11](#)
19. Li, X., Wang, H., Yi, L., Guibas, L., Abbott, A.L., Song, S.: Category-level articulated object pose estimation. Proceedings of the IEEE Conference on Computer Vision and Pattern Recognition (2020) [11](#), [12](#)
20. Li, Y., Wang, G., Ji, X., Xiang, Y., Fox, D.: Deepim: Deep iterative matching for 6d pose estimation. In: Proceedings of the European Conference on Computer Vision (ECCV). pp. 683–698 (2018) [3](#)
21. Lin, H., Liu, Z., Cheang, C., Fu, Y., Guo, G., Xue, X.: Sar-net: Shape alignment and recovery network for category-level 6d object pose and size estimation. In: Proceedings of the IEEE/CVF Conference on Computer Vision and Pattern Recognition. pp. 6707–6717 (2022) [2](#), [4](#), [11](#), [12](#)
22. Lin, J., Wei, Z., Li, Z., Xu, S., Jia, K., Li, Y.: Dualposenet: Category-level 6d object pose and size estimation using dual pose network with refined learning of pose consistency. In: Proceedings of the IEEE/CVF International Conference on Computer Vision. pp. 3560–3569 (2021) [2](#), [11](#), [12](#)
23. Lin, Y., Tremblay, J., Tyree, S., Vela, P.A., Birchfield, S.: Keypoint-based category-level object pose tracking from an rgb sequence with uncertainty estimation. In: 2022 International Conference on Robotics and Automation (ICRA). pp. 1258–1264. IEEE (2022) [4](#)
24. Liu, L., Xu, W., Fu, H., Qian, S., Yu, Q., Han, Y., Lu, C.: Akb-48: A real-world articulated object knowledge base. In: Proceedings of the IEEE/CVF Conference on Computer Vision and Pattern Recognition. pp. 14809–14818 (2022) [5](#)
25. Liu, Y., Liu, Y., Jiang, C., Lyu, K., Wan, W., Shen, H., Liang, B., Fu, Z., Wang, H., Yi, L.: Hoi4d: A 4d egocentric dataset for category-level human-object interaction. In: Proceedings of the IEEE/CVF Conference on Computer Vision and Pattern Recognition. pp. 21013–21022 (2022) [3](#), [4](#)
26. Pérez, P., Gangnet, M., Blake, A.: Poisson image editing. In: Seminal Graphics Papers: Pushing the Boundaries, Volume 2, pp. 577–582 (2023) [7](#)
27. Reizenstein, J., Shapovalov, R., Henzler, P., Sbordone, L., Labatut, P., Novotny, D.: Common objects in 3d: Large-scale learning and evaluation of real-life 3d category reconstruction. In: Proceedings of the IEEE/CVF International Conference on Computer Vision. pp. 10901–10911 (2021) [3](#), [4](#)
28. Sarlin, P.E., DeTone, D., Malisiewicz, T., Rabinovich, A.: Superglue: Learning feature matching with graph neural networks. In: Proceedings of the IEEE/CVF conference on computer vision and pattern recognition. pp. 4938–4947 (2020) [6](#)
29. Stoiber, M., Elsayed, M., Reichert, A.E., Steidle, F., Lee, D., Triebel, R.: Fusing visual appearance and geometry for multi-modality 6dof object tracking. arXiv preprint arXiv:2302.11458 (2023) [4](#)
30. Stoiber, M., Sundermeyer, M., Triebel, R.: Iterative corresponding geometry: Fusing region and depth for highly efficient 3d tracking of textureless objects. In: Proceedings of the IEEE/CVF Conference on Computer Vision and Pattern Recognition. pp. 6855–6865 (2022) [4](#), [14](#)
31. Sun, X., Wu, J., Zhang, X., Zhang, Z., Zhang, C., Xue, T., Tenenbaum, J.B., Freeman, W.T.: Pix3d: Dataset and methods for single-image 3d shape modeling.

- In: Proceedings of the IEEE conference on computer vision and pattern recognition. pp. 2974–2983 (2018) [3](#), [4](#)
32. Tjaden, H., Schwanecke, U., Schömer, E., Cremers, D.: A region-based gauss-newton approach to real-time monocular multiple object tracking. *IEEE transactions on pattern analysis and machine intelligence* **41**(8), 1797–1812 (2018) [4](#), [14](#)
 33. Wang, C., Martín-Martín, R., Xu, D., Lv, J., Lu, C., Fei-Fei, L., Savarese, S., Zhu, Y.: 6-pack: Category-level 6d pose tracker with anchor-based keypoints. In: 2020 IEEE International Conference on Robotics and Automation (ICRA). pp. 10059–10066. IEEE (2020) [4](#), [13](#), [14](#)
 34. Wang, C., Xu, D., Zhu, Y., Martín-Martín, R., Lu, C., Fei-Fei, L., Savarese, S.: Densfusion: 6d object pose estimation by iterative dense fusion. In: Proceedings of the IEEE/CVF conference on computer vision and pattern recognition. pp. 3343–3352 (2019) [3](#), [4](#), [14](#)
 35. Wang, G., Manhardt, F., Tombari, F., Ji, X.: GDR-Net: Geometry-guided direct regression network for monocular 6d object pose estimation. In: IEEE/CVF Conference on Computer Vision and Pattern Recognition (CVPR). pp. 16611–16621 (June 2021) [3](#), [11](#)
 36. Wang, H., Sridhar, S., Huang, J., Valentin, J., Song, S., Guibas, L.J.: Normalized object coordinate space for category-level 6d object pose and size estimation. In: Proceedings of the IEEE/CVF Conference on Computer Vision and Pattern Recognition. pp. 2642–2651 (2019) [2](#), [4](#), [6](#), [11](#), [12](#)
 37. Wen, B., Bekris, K.: Bundletrack: 6d pose tracking for novel objects without instance or category-level 3d models. In: 2021 IEEE/RSJ International Conference on Intelligent Robots and Systems (IROS). pp. 8067–8074. IEEE (2021) [4](#), [7](#), [14](#), [15](#)
 38. Wen, B., Mitash, C., Ren, B., Bekris, K.E.: se (3)-tracknet: Data-driven 6d pose tracking by calibrating image residuals in synthetic domains. In: 2020 IEEE/RSJ International Conference on Intelligent Robots and Systems (IROS). pp. 10367–10373. IEEE (2020) [4](#)
 39. Weng, Y., Wang, H., Zhou, Q., Qin, Y., Duan, Y., Fan, Q., Chen, B., Su, H., Guibas, L.J.: Captra: Category-level pose tracking for rigid and articulated objects from point clouds. In: Proceedings of the IEEE/CVF International Conference on Computer Vision. pp. 13209–13218 (2021) [5](#), [14](#)
 40. Xiang, Y., Schmidt, T., Narayanan, V., Fox, D.: Posecnn: A convolutional neural network for 6d object pose estimation in cluttered scenes. arXiv preprint arXiv:1711.00199 (2017) [2](#), [3](#), [4](#), [14](#)
 41. You, Y., He, W., Liu, J., Xiong, H., Wang, W., Lu, C.: Cppf++: Uncertainty-aware sim2real object pose estimation by vote aggregation. arXiv preprint arXiv:2211.13398 (2022) [11](#), [12](#)
 42. Ze, Y., Wang, X.: Category-level 6d object pose estimation in the wild: A semi-supervised learning approach and a new dataset. *Advances in Neural Information Processing Systems* **35**, 27469–27483 (2022) [4](#)
 43. Zheng, L., Wang, C., Sun, Y., Dasgupta, E., Chen, H., Leonardis, A., Zhang, W., Chang, H.J.: Hs-pose: Hybrid scope feature extraction for category-level object pose estimation. In: Proceedings of the IEEE/CVF Conference on Computer Vision and Pattern Recognition. pp. 17163–17173 (2023) [2](#), [4](#), [11](#), [12](#)